Zonal winds at high latitudes on Venus: An improved application of cyclostrophic balance to Venus Express observations

Zonal winds at high latitudes on Venus: an improved application of cyclostrophic balance to Venus Express observations

João M. Mendonça [a], Peter L. Read [a], Colin F. Wilson [a] and Stephen R. Lewis [b]

[a] *Department of Physics, University of Oxford, Clarendon Laboratory, Parks Road, Oxford, U.K.*

[b] *Department of Physics and Astronomy, The Open University, Walton Hall, Milton Keynes, U.K.*

Number of pages: 24

Number of tables: 0

Number of figures:12

Preprint submitted to Icarus *12 May 2011*

Proposed Running Head:

Polar atmospheric circulation of Venus.

Please send Editorial Correspondence to:

João M. Mendonça

University of Oxford

Atmospheric, Oceanic and Planetary Physics

Clarendon Laboratory

Parks Road

Oxford, OX1 3PU

U.K.

Email: mendonca@atm.ox.ac.uk

Phone: +44 (0) 1865 272933

Fax: +44 (0) 1865 272923

ABSTRACT

Recent retrievals of zonal thermal winds obtained in a cyclostrophic regime on Venus are generally consistent with cloud tracking measurements at mid-latitudes, but become unphysical in polar regions where the values obtained above the clouds are often less than or close to zero. Using a global atmospheric model, we show that the main source of errors that appear in the polar regions when retrieving the zonal thermal winds, is most likely due to uncertainties on the zonal wind intensity in the choice of the lower boundary condition.

Here we suggest a new and robust method to better estimate the lower boundary condition for high latitudes, thereby improving the retrieved thermal zonal winds throughout the high latitudes middle atmosphere. This new method is applied to temperature fields derived from Visible and Infrared Thermal Imaging Spectrometer (VIRTIS) data on board the Venus Express spacecraft. We obtain a thermal zonal wind field that is in better agreement with other, more direct methods based on either retrieving the zonal winds from cloud tracking or from direct measurements of the meridional slope of pressure surfaces.

Keywords: Venus ; Venus, atmosphere ; Atmospheres, dynamics

1 Introduction

The retrieval of the zonal thermal winds from temperature measurements in Venus' atmosphere has been shown to be a very powerful tool to study the dynamics of the atmosphere in the absence of direct wind measurements (Chub and Iakovlev 1980; Seiff 1983; Newman et al. 1984; Limaye 1985; Roos-Serote et al. 1995; Zasova et al. 2007; Piccialli et al. 2008; Piccialli et al. 2011). These methods are based on a particular dynamical balance that characterises quite well the nature of the circulation in the Venus mesosphere (between 55 and 100 km altitude). On Earth, which is a relatively rapidly rotating planet (with small zonal Rossby number), the geostrophic approximation is often assumed for large-scale atmospheric motions, where the pressure gradient term is approximately balanced by the Coriolis acceleration. In the mesosphere of Venus, this approximation fails because in those layers of the atmosphere we have strong winds overlying a slowly rotating planet. In this case, the cyclostrophic approximation, in which the centrifugal acceleration balances the geopotential gradient term, may be used (Leovy 1973). From the meridional component of the equation of motion in a planetary atmosphere, we can obtain the cyclostrophic thermal wind equation from the balance of these two terms,

$$\frac{u^2 \tan\phi}{a} = -\frac{1}{a}\frac{\partial \Phi}{\partial \phi}, \tag{1}$$

where ϕ is latitude, u the zonal wind velocity, a the radius of the planet and Φ is the geopotential. Differentiating in altitude each side of the equation and assuming a hydrostatic balance, this can be simply written in pressure

coordinates, following Newman et al. (1984) and Piccialli et al. (2008), as:

$$2u\frac{\partial u}{\partial \zeta} = -\frac{R}{\tan\phi}\frac{\partial T}{\partial \phi}|_{p=const}, \tag{2}$$

where R is the gas constant and T the temperature. The variable ζ is defined as $-log(\frac{p}{p_o})$, where p is the pressure at each altitude level and p_o is a reference pressure.

Recent determinations of the zonal thermal winds obtained in a cyclostrophic regime are typically consistent with the cloud tracking results at mid-latitudes, but inconsistent or unphysical in the polar region, where the values obtained are less than or close to zero (e.g. Newman et al. 1984 for the north polar vortex and Piccialli et al. 2008 for the south polar vortex). Note that in this work we use the term "prograde" to refer to winds in the direction of the planet's rotation, i.e. westward. On the other hand, observations such as in Schofield and Diner (1983), Piccioni et al. (2007a) and Sánchez-Lavega et al. (2008), show clear evidence for the rotation of the polar vortex in the same direction as the global mean zonal wind, which contradicts the low or negative zonal velocities apparently retrieved from thermal winds.

In this study we investigate the likely cause of these unphysical and inaccurate thermal wind retrievals in the polar regions, using fully self-consistent simulations of Venus atmospheric circulation with a simplified general circulation model (Lee et al. 2005; Lee 2006; Lee et al. 2007). Likely causes are either due to a breakdown of cyclostrophic balance or the amplifications of observational errors in the assumed lower boundary condition of the cyclostrophic retrieval.

In the next section we briefly describe the **S**implified **G**eneral **C**irculation

Model (SGCM) used in this work. We study the full zonally averaged meridional component of the equation of motion in section 3, where we analyse the contributions of all the different terms from the SGCM's results. The aim is to clarify the dynamical nature of the circulation and, in particular, to assess the applicability of cyclostrophic balance at high latitudes.

In section 4, we study the impact of uncertainties in the lower boundary condition for the upward integration of the thermal wind equation. The high sensitivity of the "traditional" zonal thermal wind retrieval method to the lower boundary condition motivated the development of a simple method capable of recovering the zonal thermal winds mainly at high latitudes, where it is often difficult to define a reliable and accurate lower boundary condition from cloud tracking results due to the uncertainties associated with the altitudes of the clouds and zonal winds intensity. In this section we also explore the robustness of this new method for different conditions and obtain improved maps of the zonal thermal winds retrieved from a simulated temperature field to test the accuracy of the new method.

In section 5, we apply the corrected retrieval method to temperature fields obtained from the **V**isible and **I**nfrared **T**hermal **I**maging **S**pectrometer (VIRTIS) data on board the Venus Express spacecraft, to obtain a new zonal wind field which we compare with other recent observational results.

Finally, concluding remarks are presented in section 6.

2 Simplified General Circulation Model

The SGCM used here is called the **O**xford **P**lanetary **U**nified (Model) **S**ystem for **V**enus (OPUS-V), and obtains a dynamically self-consistent representation of the circulation of the Venus' atmosphere (Lee et al. 2005; Lee 2006; Lee et al. 2007).

The model uses physical and dynamical parameters corresponding to Venus (Colin 1983; Williams 2003), and simplified parameterisations for radiative forcing and boundary layer dissipation. It is based on the dynamical core of the UK Hadley Centre Unified Model (Cullen et al., 1992) and configured on an Arakawa B grid (Arakawa and Lamb, 1981), using a 5°x5° horizontal resolution, covering the entire global domain with 32 vertical levels (with a maximum vertical grid spacing of ∼3.5 km). The atmosphere modelled extends from the surface to an altitude of around 90 km (∼0.5hPa). The thermal forcing scheme used is not based on a full radiative transfer model but on a simplified formulation using a linear temperature relaxation scheme towards a prescribed temperature field that is a function only of latitude and height (pressure). The latter is derived from the superposition of a global-averaged reference temperature profile, obtained from Pioneer Venus probe data (Seiff et al., 1980), plus a perturbation that is function of latitude and pressure that determines the equator-to-pole thermal contrast at each altitude. This structure is chosen to produce a peak in solar heating within the altitude range of the observed cloud deck (Tomasko et al. 1985; Lee 2006; Lee et al. 2007). The mechanical interaction of the atmosphere with the surface was modelled by a simple boundary layer drag scheme with a linearised Rayleigh friction parameterisation. In the three upper most layers a sponge layer is included,

with Rayleigh friction acting to damp horizontal *eddy* winds to zero (though not the zonal mean flow; Lee 2006; Lee et al. 2007).

Using this SGCM for Venus, it is possible to reproduce a substantially super-rotating atmosphere via the well known GRW mechanism (Gierasch 1975; Rossow and Williams 1979) without any non-physical forcing, diurnal or seasonal cycles. The horizontal equatorward eddy transport of momentum at 40-80 km is responsible for maintaining the equatorial super-rotation (Lee 2006; Lee et al. 2007). The model produces equatorial Kelvin and Mixed-Rossby-Gravity (MRG) waves spontaneously. Lee (2006) found that the MRG waves contribute to equatorward momentum transport and help maintaining the equatorial super-rotation. The model also simulates, among other phenomena, a "cold collar" in the middle atmosphere and a warm pole in the upper atmosphere, although with somewhat weaker amplitudes than observed. Further details can be found in Lee (2006) and Lee et al. (2007).

2.1 Base Run

A reference simulation used for the present study was integrated for 4.1×10^4 (Earth) days, with a time-step of 10 minutes and did not include a diurnal cycle or surface topography. The numerical model integration started with the atmosphere at rest with respect to the underlying planet, a surface pressure of 92.0 bar and a vertical temperature profile very close to the VIRA (Venus International Reference Atmosphere) model for each grid point. Fig. 1 shows meridional cross-sections of the zonal winds and a temperature map that were zonally and time averaged in the last hour of the simulation. The atmospheric circulation is close to being statistically steady, although it does exhibit a

slight increasing tendency in the kinetic energy of the global atmosphere even after more than 100 Earth years of spin-up.

The zonal winds produced by the model are illustrated in Fig. 1(a) for the Northern hemisphere (the pattern is similar to the Southern hemisphere). A jet structure is seen to form at roughly 450 hPa and 67.5^o N latitude with a maximum of around 47.5 $\mathrm{m\,s^{-1}}$ (about a half of the wind strength observed by e.g. Schubert 1983). The zonal wind speed in the equatorial mesosphere region is slower than in the mid-latitudes but it is still prograde and super-rotating with respect to the solid planet.

The temperature map in Fig. 1(b) shows two regions with very different gradients of temperature towards the pole. Near the bottom of the jet there is a negative gradient (poleward decreasing) while near the top a positive gradient (poleward increasing) is formed. From the temperature map it is possible to observe in the polar regions of the atmosphere (around 75^o N latitude), between 200 hPa and 650 hPa, colder temperatures than in the poles or the equator, which is a feature known as the "cold collar". The warm pole and the polar "cold collar" temperature structures are also observed in the Venus atmosphere (Taylor et al., 1979), although with higher magnitude than produced in the model.

3 Zonally averaged meridional equation of motion

The full zonally averaged meridional component of the equation of motion on a spherical planet of radius, a, and angular velocity, Ω, is used in this work as a basis for studying the respective contribution of each term and

to examine the qualitative validity of the cyclostrophic approximation. The equation is defined using an Eulerian-mean (denoted by $\bar{u}$ for variable u), at fixed latitude ϕ, time t and pressure level p,

$$\underbrace{\bar{u^2}a^{-1}\tan\phi}_{[\mathrm{A}]} - \underbrace{\bar{u}f}_{[\mathrm{B}]} + \underbrace{a^{-1}\bar{\Phi}_\phi}_{[\mathrm{C}]} = -\underbrace{(a\cos\phi)^{-1}(\overline{v'^2}\cos\phi)_\phi}_{[\mathrm{D}]} - \underbrace{\overline{u'^2}a^{-1}\tan\phi}_{[\mathrm{E}]} + \mathscr{R} \quad (3)$$

where the subscript denotes a partial derivative, [A] represents the centrifugal acceleration, [B] the Coriolis acceleration, [C] the geopotential gradient, [D] and [E] the quadratic terms in disturbance variables which are written on the right hand side and represent the "rectified eddy-forcing" terms (e.g. Andrews et al. 1987) and $\mathscr{R}$ the residual. The eddy terms govern the interaction of the zonal mean flow with superimposed disturbances, which could have a very important effect on the zonal mean circulation in regions of strong eddy activity. The residual term $\mathscr{R}$ quantifies the remaining terms neglected in this approximation and represents residual time dependence and other effects (such as frictional processes) not included explicitly in Eq. (3).

The magnitude of each of the terms in Eq. (3), averaged over an hour in the model run, are plotted in Fig. 2. It can be seen that the equation is dominated mainly by two terms: the centrifugal acceleration [A] and the geopotential gradient [C], indicating that the cyclostrophic balance is accurate to better than 20% almost everywhere. However, the residual $\mathscr{R}$ is not negligible in the polar region and becomes more significant for higher altitudes above the jet. It includes all the terms that we are neglecting and seems to be more relevant in the "turbulent" regions where eddy activity is strong. An important contribution to the residual is almost certainly due to the term $\frac{\partial v}{\partial t}$ related to the flow variability, especially in the polar regions. The two eddy terms [D]

and [E], do not have negligible magnitude in the polar region and seem to be related to the "turbulent" zone near the jets as well. A latitude-pressure map of the two main eddy terms [D] and [E] for this case are shown in Fig. 3. Both terms have important contributions at high latitudes, stronger in the jet region (around 300 hPa), and apparently leading to a partial breakdown of the cyclostrophic balance. In Fig. 2, we can see that the eddy terms can have a larger magnitude than the zonal mean cyclostrophic terms for latitudes higher than 80^o.

Upon averaging each term of Eq. 3 for a longer time (60 Earth days), we reduce the contribution of the "turbulent" term $\frac{\partial v}{\partial t}$. In Fig. 4 we show the results obtained. We see a smoother residual profile for the two altitudes sampled here (100 hPa and 952 hPa), which is now nearly zero almost everywhere but with a slight increase towards the pole. A pure cyclostrophic balance is, in general therefore, a good approximation to describe the time- and zonal-mean atmospheric circulation, however, for latitudes higher than 80^o the significant total contribution of the eddy (dashed-dot line) terms can lead to a partial breakdown of the cyclostrophic approximation, as mentioned before. The benefit of neglecting the two eddy terms is that it simplifies the method to retrieve the thermal zonal winds. A more complete retrieval method would need to be based on a combination of the cyclostrophic balance terms and an eddy diffusion parameterisation (e.g. Luz et al. 2003). However, we show below that this is not the main source of error present in cyclostrophic wind retrievals, and that an alternative approach based on applying a simple dynamical constraint to pure cyclostrophic balance, can still yield good estimates of zonal winds at high latitudes.

4 Retrieving the Thermal Zonal Winds in Venus Model Simulations

The zonal thermal wind equation applied to the Venus mesosphere, Eq. (2), can be used to obtain the zonal velocity u given the temperature field, provided that the cyclostrophic balance condition is valid. Here it is assumed that the solutions for u are always positive (prograde). One of the main difficulties in this method is related to finding an appropriate lower boundary condition to be used in the upward integration. Cloud tracking techniques have typically been used to estimate the winds at the lower boundary, but this method is often not very accurate at high latitudes because of a lack of clearly defined features in cloud images and uncertainties in defining the cloud top altitude.

We suggest here, therefore, a new method to better estimate the lower boundary condition in the polar region. This method complements previous work on zonal thermal wind retrievals and it comprises additional iterations. Our new method to retrieve the zonal winds has the following structure:

(1) Integrate the thermal wind equation upwards using Eq. (2), starting from a first initial guess for the lower boundary.

(2) Correct the circumpolar winds at the top of the model domain (p_{top}) to be consistent with a solid body rotation profile (with the form $\frac{u_0(p_{top},\phi_0)}{\cos\phi_0}\cos\phi$) in the latitude region starting from the position of the jet core (ϕ_0), up to the pole. The position of the jet core is defined here to be 5 degrees lower in latitude than the position of the zonal thermal wind maximum (equivalent to the latitudinal resolution of the SGCM).

(3) Integrate Eq. (2) *downwards* with the new upper boundary condition.

Here we are effectively estimating a new lower boundary condition, which fits better with the conditions of a Venus' mesosphere circulation.

The imposition of a mean atmospheric vortex in the Venus mesosphere approximating to a solid body rotation close to the pole, is plausible for several reasons. The zonally flow is approximately angular momentum conserving at low latitudes but this cannot hold up to the pole, otherwise the zonal winds would be unrealisticaly large, increasing with the inverse of cos ϕ. The circumpolar jet is typically barotropically unstable, and barotropic eddies associated with the jet in the Venus atmosphere tend to mix towards a state of approximately uniform vorticity ξ (Schubert et al. 1999). In cylindrical polar coordinates centred on the rotation axis, uniform axial vorticity corresponds exactly to solid body rotation at angular velocity $w = \frac{\xi}{2}$. This equivalence is not exact in spherical polar coordinates, but is a close approximation near the pole, broadly similar to the approximate Rankine vortex infered from observations on Venus (Limaye 2007). A near-solid body rotation is also in line with the pattern of zonal winds most commonly obtained by the SGCM in the polar region for altitudes above the jet.

Results in Fig. 5 were obtained from the upward integration of Eq. (2) using an ensemble of different lower boundary conditions prescribed to have the following form:

$$U_o = (a \times \mathrm{sech}(\frac{|\phi| - b}{c}) + d) \times cos(\phi). \tag{4}$$

where a, b, c and d are free parameters and ϕ the latitude. This equation was firstly used by Newman et al. (1984), to fit the DLBI measured winds at about 42 km from Counselman et al. (1980). The different parameters, de-

termine different characteristics of a zonal wind profile, where a, b and c are the magnitude, latitude position and width of the jet, and d the zonal wind flow at low latitudes. The lower boundary is applied at a pressure level around 3000 hPa. In these experiments the parameter a was varied randomly over the interval $[0-300]\mathrm{m\,s^{-1}}$, b on $[82.5^o-87.5^o]$, c on $[8-12]$ and d on $[10-40]\mathrm{m\,s^{-1}}$ with uniform probability. For the results in Fig. 5, we used a temperature field that was zonally and time averaged (over 60 Earth days) from the SGCM, and the top of the model domain was fixed at 30 hPa. The dashed line represents the standard deviation of the zonal winds profile obtained at the top of the domain over the standard deviation of the initial profiles for the lower boundary condition. From this line it is possible to conclude the high sensitivity (values higher than one) of the upward integration to the values chosen for the lower boundary.The solid line corresponds to the standard deviation of the profile which is "corrected" to have the form of a solid body rotation at the top of the domain as explained in the step (2) of the new method, over the standard deviation of the initial profiles for lower boundary condition. The variability of this profile is weaker than the one represented by the dashed line. The important conclusion from Fig. 5 is that the results from the upward integration are very sensitive to changes in the lower boundary condition in the polar region. The use of an inappropriate lower boundary condition is therefore clearly likely to produce inaccurate results, even with a well constrained thermal field. This problem can be improved with the new method proposed above.

In order to study the reliability and robustness of the new method as a means of better estimating the winds at the lower boundary in the polar region, we study the results using an ensemble of initial lower boundary profiles. The large number of initial guesses for the lower boundary condition was obtained

using the same method and parameters used for Fig. 5.

In Fig. 6 the top and the bottom of the temperature field studied were set again at 30 hPa and 3000 hPa respectively. This experiment shows the effect of different time averaging periods on the final result of the estimation of the lower boundary in the polar region. As expected, the longer time averaging of the temperature field gives better results, because we are closer to the conditions of a pure cyclostrophic regime. The zonal winds near the jet region are being underestimated for shorter time periods. The dashed line in the figure represents the zonally- and time-averaged zonal winds obtained by the SGCM at the pressure level where the lower boundary condition is defined. Note that the retrieved results from the initial latitude position of the jet up to the pole occupy a small range of values that are always close to the "true" values (indicated by the dashed line). The small values of the ratio of the final result's standard deviation to the standard deviation of the initial guesses (solid line), suggest that the final best estimate is well constrained and is not significantly affected by different initial guess profiles.

For the experiments shown in Fig. 7, we changed the top pressure level where the suggested method is applied. Six different top pressures were tested: 2.1 hPa, 4.6 hPa, 9.8 hPa, 21 hPa, 45 hPa and 100 hPa. The time period for averaging the zonally averaged temperature field from the SGCM was 60 Earth days. The accuracy of the results depends to some extent on where the top is defined. For atmospheric pressures below 21 hPa the values of the zonal winds at the lower boundary tend to be overestimated near the jet region. The zonal winds in the SGCM at this region appear to decrease faster with latitude than for solid body rotation between 65^o and 80^o. Defining the top for pressure levels deeper than 21 hPa, leads to an underestimate of the value

of the lower boundary obtained, because we are then forcing the zonal winds near the latitude position of the jet core to decrease more rapidly with latitude than observed in the original SGCM results (Fig. 8(a)). The pressure layer at 21 hPa is where the zonal winds better approximate to a solid body rotation, although the meridional motions in the atmosphere are very weak. Above 21 hPa there is a weak polarward circulation and equatorward below 21 hPa, which weakens the solid body rotation assumption.

In addition, the values of zonal wind speeds at the lower boundary estimated for latitudes higher than 80^o, are usually underestimated due to the presence of a non-negligible residual term and the two eddy terms, as shown in Fig. 4. The standard deviation of the final results is larger in the latitudes farthest from the pole, due to the high sensitivity of u_o, that is used to reconstruct the profiles $\frac{u_0(p_{top},\phi_0)}{\cos\phi_0}\cos\phi$ (solid body rotation's profile) at the top of the model domain. This implies that for better results when retrieving the thermal zonal winds, one needs to constrain the flows to low latitudes.

In general, the new method used to estimate the lower boundary condition for latitudes higher than the centre of the jet, produces results very close to the expected profile. The duration of time averaging affects the results, with longer periods leading to better results due to the improved accuracy of the assumed cyclostrophic balance in characterising the large scale flow for these cases. The suggested method is easy to apply and reduces the difficulties due to inaccurate initial conditions for the upward integration of the thermal wind equation.

On further exploring Eq. (2), we study the accuracy of this method to retrieve the entire zonal thermal wind map from a zonally and time averaged

temperature field obtained at the end of SGCM simulation (averaged for 60 Earth days). Fig. 8 shows the zonal thermal wind maps retrieved using three different lower boundary conditions:

(1) A zonally and time averaged zonal winds profile obtained by the SGCM.
(2) One with the typical shape assumed before but which deliberately underestimates the zonal wind velocities in the polar regions (Eq. (4) with $a = 50\ \mathrm{m\,s^{-1}}$, $b = 70^o$, $c = 10$ and $d = 20\ \mathrm{m\,s^{-1}}$)
(3) Using the method suggested previously to better estimate the lower boundary in the polar region applied to (2).

Fig. 8(b) shows the thermal zonal winds obtained using the best answer for the lower boundary, case (1), which obtains in general, zonal winds magnitudes close to the ones expected from the SGCM results (Fig. 8(a)). As expected, the use of an inappropriate lower boundary condition for case (2), underestimates the values in the polar region and produces incorrect results at all heights. The magnitude of the zonal thermal winds from Fig. 8(c) are in general smaller than the zonal winds produced by the SGCM (Fig. 8(a)). The application of the new method to estimate the lower boundary condition, reconstructs the zonal wind field in the region from 65^o latitude up to the pole for all altitudes (Fig. 8(d)), converging in results close to the ones represented by Fig. 8(b) that uses the best lower boundary estimation. The maximum of the recovered wind velocity at the jet core is $46.0\ \mathrm{m\,s^{-1}}$ at 72.5^o latitude, which is almost identical to the one produced by the SGCM, $\bar{u} = 46.5\ \mathrm{m\,s^{-1}}$ at 72.5^o. The final zonal thermal wind field is in better agreement with the zonal winds from the SGCM than the case (2), despite using a general, and not very accurate, first guess for the lower boundary profile.

5 A Map of Zonal Thermal Winds obtained from VIRTIS Data

We will now study the thermal zonal winds obtained from the latitude-pressure mesosphere temperature map for a particular local time, retrieved by the mapping IR channels of the **V**isual and **I**nfrared **T**hermal **I**maging **S**pectrometer (VIRTIS-M) on board the Venus Express spacecraft (Piccioni et al. 2007b).

The latitude-pressure temperature map used is part of the compilation of temperature retrievals from Grassi et al. (2010), which are roughly equivalent to the previous long time average results using the SGCM temperature fields. The time averaging attenuates the intensity of time varying dynamical flows impressed in the temperature map. The different local times correspond to different thermal structures that drives changes in the atmospheric circulation, such as the position of the jet (Held and Hou 1980 and Newman and Leovy 1992). The map covers the domain 1-100 hPa from 45^o latitude up to the pole in the Southern hemisphere for 2400LT. The overall uncertainty in the retrieved temperature in this region does not exceed 4 K and is better than 1 K between 7 and 70 hPa. The map of temperatures is shown in Fig. 9, where it is possible to observe the "cold collar" at 65^oS and the temperatures increasing monotonically towards the pole for altitudes above the pressure level 12.6 hPa.

The zonal thermal winds shown in Fig. 10 are obtained from the temperature map using Eq. (2). Fig. 10(a) was obtained just from a single upward-integration of the Eq. (2) from a lower boundary condition that was prescribed to have the form given in Eq. (4) with $a = 52$ m s^{-1}, $b = 56^o$, $c = 9$ and $d = 86$ m s^{-1}. This profile was constrained using the one presented in Piccialli et al. (2008) for a surface pressure altitude of 275 hPa. The values for a and d are

larger by $\sim 15\%$ in our work, which were estimated from their zonal thermal wind retrieval maps (for altitudes below the pressure level 100 hPa the zonal wind speeds decrease with pressure). We did not set the lower boundary at 275hPa because we do not have temperature data available below 100 hPa. For each level the latitudinal profile of the temperature data was smoothed using a cubic spline method with a smoothing parameter of 0.01, to facilitate the evaluation of $[\partial T/\partial \phi]_{p=const}$. This procedure can affect the pattern of the zonal thermal winds, however, if we artificially create thermal structures not consistent with the real Venus meteorology. Fig. 10(a) shows the zonal thermal winds obtained from VIRTIS data, with a mid-latitude jet reaching a maximum of 108 ± 7 m s^{-1} at a latitude of -48 ± 5^o. As observed in other studies (Newman et al. 1984; Piccialli et al. 2008), the zonal thermal winds in the polar region appear to be weaker than what would be expected from direct observation of the clouds in the polar vortex (Piccioni et al. 2007a). The clumpy dark region (latitudes higher than 65^o) is related to integration problems since we cannot determine if the winds reverse direction.

In Fig. 10(b) we use the new method described in section 4 to calculate zonal thermal winds from a VIRTIS data set. This method, which estimates the lower boundary condition, increases the zonal winds in the region where it is applied (for all altitudes from the latitude position of the jet core up to the pole). In this case the maximum velocity in the jet is still 108 ± 7 m s^{-1} at -48 ± 5^o latitude.

A modified equation for the lower boundary was also tested, this profile increases the final thermal zonal winds mainly at mid-latitudes, replacing $d = 86$ m s^{-1} by $d = 105$ m s^{-1}. Here we are assuming stronger winds in the low/mid-latitudes, which were constrained using the Sánchez-Lavega et al.

(2008) results. Retrieving the thermal zonal winds using the method to estimate the lower boundary and the new first initial guess, we see that slightly stronger mean mid-latitude winds are produced (Fig. 10(c)), when compared with Figs. 10(a) and 10(b). The maximum wind speed is now $116 \pm 7 m\,s^{-1}$ at -48 $\pm$ 5^o. The results derived here are in good agreement with the results obtained by Zasova et al. (2000), who obtained a jet centred at around 50^{o}S with u $\sim 110 m\,s^{-1}$. Other works obtained roughly the same position but different maximum wind speeds, such as $\sim 160 m\,s^{-1}$ from Newman et al. (1984), $\sim 90 m\,s^{-1}$ from Piccialli et al. (2008) and more recently $\sim 140 m\,s^{-1}$ from Piccialli et al. (2011).

The retrieved zonal thermal winds start to converge for latitudes higher than 70^o when the same technique to obtain the lower boundary but different initial guesses is used (e.g. the black solid line and solid circles in Fig. 12). It is also important to point out the large horizontal shear in these last results close to the pole. This is consistent with barotropic instability becoming important, influencing the dynamics of the polar vortices.

The uncertainties in the jet magnitude and position presented were estimated using a Monte-Carlo method, where the temperature for each point varied with uniform probability within $\pm 4K$, before fitting the temperature profiles for each level (10^4 steps). The 4 Kelvin is indicated in Grassi et al. (2010) and previously in this paper, as the maximum total error in the temperature retrievals throughout the entire range 100.0-1.0 hPa (65-85 km). The uncertainty is computed for each particular lower boundary condition, and is the root mean square of all standard deviations in each point, including implicitly the error of the fit. The error in latitude is the standard deviation of the position of the maximum magnitude in the wind map after running all the

Monte-Carlo steps.

Limaye (1985), and more recently Piccialli et al. (2011), also used a second method that obtains the zonal winds using the cyclostrophic approximation directly via Eq. (1) from the meridional slope of the pressure surfaces. This method has the advantage of not requiring a vertical integration, thereby avoiding problems with the choice of the lower boundary condition. However, this method requires measurement of the height of pressure surfaces, which is obtained by radio occultation, so profiles are few in number and widely separated in space and time. Nevertheless, the results obtained with this method show strong prograde zonal winds in the polar region in agreement with our method, as showed in Fig. 11 in dashed-dot line for an altitude of $\sim$ 65 km (100 hPa). The solid line in Fig. 11 represents the zonal thermal wind obtained using our new method with the previous indicated lower boundary condition with d = $105 m\,s^{-1}$. For latitudes lower than 70^o the zonal winds obtained by Piccialli et al. (2011) are in general larger, reaching $\sim 120 m\,s^{-1}$ at 50^o, contrasting with our thermal zonal wind magnitude of $95 m\,s^{-1}$.

The comparison with cloud-tracked wind measurements acquired also from Venus Express, allow us a first validation of our method based on a cyclostrophic balance. The profiles used and presented in Fig. 11, are the VIRTIS near infrared cloud-tracked winds obtained by Sánchez-Lavega et al. (2008) at $\sim 66 km$ (black circles) and the VIRTIS UV paired method at $\sim 70 km$ from Moissl et al. (2009) (unfilled circles). These two profiles are in general in good agreement between them, being the main differences: the more pronounced peak in the zonal winds in Sánchez-Lavega et al. (2008) results reaching $\sim 110 m\,s^{-1}$ and the larger zonal wind around $35 m\,s^{-1}$ at -85^o latitude derived from VIRTIS UV images. The differences between these results and

the ones obtained using our method at high latitudes are clear, and can be related with difficulties in both methods. One important source of error in the cloud-tracked methods is the definition of the altitude of the cloud top map. In Ignatiev et al. (2009), simultaneous observations of VIRTIS and Venus Monitoring Camera (VMC) onboard the Venus Express spacecraft, mapped the mean cloud top altitude as a function of latitude and local time. It is clear from these results the presence of a depression in the cloud top altitudes for latitudes higher than 50^o (from $\sim$ 74 km to 63-69 km), which can imply that the zonal winds at high latitudes obtained by cloud-tracked methods correspond to altitudes deeper in the atmosphere. On the other hand, our method is based on a cyclostrophic approximation that might be weaken by the presence of the residual term presented before and the eddy fluxes.

In Fig. 12, we explore how the method to estimate the lower boundary is sensitive to the initial guess (analogous to the work done using SGCM data). The initial guesses again have the form of Eq. (4). We explored 2.5×10^5 different random profiles with the same probability distribution for each parameter as what was used in the previous paragraph. The mean profile is represented by the dashed line in Fig. 12. The embedded plot in Fig. 12 represents the ratio of the standard deviation of the final results (shaded region) to the standard deviation of the initial guesses (as in the SGCM results section). The low numbers obtained indicate that the method to estimate the zonal thermal winds from the observed temperature fields for latitudes higher than the position of the jet is weakly sensitive to changes in the initial guesses under this approach.

6 Conclusions

Previous work on thermal wind retrievals failed to obtain the zonal winds in the polar regions (latitudes higher than 70^o). In this work we find that one of the main difficulties is the use of an inaccurate lower boundary condition in the upward integration of the cyclostrophic thermal wind equation, which produces inaccurate results that propagate and amplify with the upward integration. Another minor factor is that at latitudes higher than 60^o, the presence of eddy fluxes and variance terms weaken the validity of the cyclostrophic approximation, although this source of systematic error seems to be fairly small. We have presented a new method to estimate the lower boundary from the latitude position of the jet up to the pole. The procedure was explored for different conditions, showing that it is robust to changes in the initial lower boundary guess provided the low-latitude flow is well constrained. We learned also that the method is more accurate when applied to temperature fields that are a product of long time averaging (closer to the regime of pure cyclostrophic balance). The choice of the top level of the retrieval domain can also affect the results, with the most problematic case happening when the top is defined near the jet region, leading to an underestimation of the final zonal thermal wind speed.

The new method applied to observational data is found to increase the magnitude of the winds at high latitudes, improving previous results where the values for the lower boundary at high latitudes may have been underestimated or inaccurately specified. The magnitude of the winds at latitudes higher than 70^o are now in good agreement with recent results from Piccialli et al. (2011), who use a method which computes directly the zonal winds from the evalu-

ation of the meridional slope of the pressure surfaces (removing the need to define a lower boundary condition). The results also show significant zonal wind speeds in the polar region and strong horizontal shear at the poles, in contrast to previous works that obtained weaker winds. The well-known rotation of the double-vortex (Piccioni et al., 2007a) implies significant zonal wind speed in the prograde direction as obtained in our work.

The method developed in this paper can help to better characterise the atmospheric circulation in the Venus mesosphere using the several temperature retrievals available. This new method can also be applied in conjunction with results from cloud tracking in the high-latitude region, to study and characterise winds near the altitude of the cloud top.

Acknowledgements

JM acknowledges financial support from FCT - Fundação para a Ciência e a Tecnologia (Portugal). The authors thank the Met Office for the use of the HadAM3 dynamical core in this work.

References

D. G. Andrews, J. R. Holton, and C. B. Leovy. *Middle atmosphere dynamics.* 1987.

A. Arakawa and V. R. Lamb. A potential enstrophy and energy conserving scheme for the shallow water equations. *Monthly Weather Review*, 109: 18–36, 1981.

E. V. Chub and O. I. Iakovlev. Temperature and zonal circulation of the

atmosphere of Venus based on the data of radio probe experiments. *Cosmic Research*, 18:331–336, November 1980.

L. Colin. *Venus*, pages 10–26. 1983.

C. C. Counselman, S. A. Gourevitch, R. W. King, G. B. Loriot, and E. S. Ginsberg. Zonal and meridional circulation of the lower atmosphere of Venus determined by radio interferometry. *J. Geophys. Res.*, 85:8026–8030, December 1980. doi: 10.1029/JA085iA13p08026.

M. J. P. Cullen, T. Davies, and M. H. Mawson. Conservative finite diferences schemes for a unified forecast/climate model. . *Unified Model Documentation Paper No. 10. Meteorological Office, UK.*, 1992.

P. J. Gierasch. Meridional circulation and the maintenance of the Venus atmospheric rotation. *Journal of Atmospheric Sciences*, 32:1038–1044, June 1975.

D. Grassi, A. Migliorini, L. Montabone, S. Lebonnois, A. Cardesìn-Moinelo, G. Piccioni, P. Drossart, and L. V. Zasova. Thermal structure of Venusian nighttime mesosphere as observed by VIRTIS-Venus Express. *Journal of Geophysical Research (Planets)*, 115:9007, September 2010.

I. M. Held and A. Y. Hou. Nonlinear Axially Symmetric Circulations in a Nearly Inviscid Atmosphere. *Journal of Atmospheric Sciences*, 37:515–533, March 1980. doi: 10.1175/1520-0469(1980)037¡0515:NASCIA¿2.0.CO;2.

N. I. Ignatiev, D. V. Titov, G. Piccioni, P. Drossart, W. J. Markiewicz, V. Cottini, T. Roatsch, M. Almeida, and N. Manoel. Altimetry of the Venus cloud tops from the Venus Express observations. *Journal of Geophysical Research (Planets)*, 114:E00B43, August 2009. doi: 10.1029/2008JE003320.

C. Lee. *Modelling of the Atmosphere of Venus*. PhD thesis, Oxford University, 2006.

C. Lee, S. R. Lewis, and P. L. Read. A numerical model of the atmosphere of

Venus. *Advances in Space Research*, 36:2142–2145, 2005.

C. Lee, S. R. Lewis, and P. L. Read. Superrotation in a Venus general circulation model. *Journal of Geophysical Research (Planets)*, 112(E11):4–+, April 2007.

C. B. Leovy. Rotation of the upper atmosphere of Venus. *Journal of Atmospheric Sciences*, 30:1218–1220, 1973.

S. S. Limaye. Venus atmospheric circulation - Observations and implications of the thermal structure. *Advances in Space Research*, 5:51–62, 1985.

S. S. Limaye. Venus atmospheric circulation: Known and unknown. *Journal of Geophysical Research (Planets)*, 112:4, April 2007.

D. Luz, F. Hourdin, P. Rannou, and S. Lebonnois. Latitudinal transport by barotropic waves in Titan's stratosphere. II. Results from a coupled dynamics-microphysics-photochemistry GCM. *Icarus*, 166:343–358, December 2003.

R. Moissl, I. Khatuntsev, S. S. Limaye, D. V. Titov, W. J. Markiewicz, N. I. Ignatiev, T. Roatsch, K.-D. Matz, R. Jaumann, M. Almeida, G. Portyankina, T. Behnke, and S. F. Hviid. Venus cloud top winds from tracking UV features in Venus Monitoring Camera images. *Journal of Geophysical Research (Planets)*, 114:0–+, March 2009. doi: 10.1029/2008JE003117.

M. Newman and C. Leovy. Maintenance of strong rotational winds in Venus' middle atmosphere by thermal tides. *Science*, 257:647–650, July 1992. doi: 10.1126/science.257.5070.647.

M. Newman, G. Schubert, A. J. Kliore, and I. R. Patel. Zonal winds in the middle atmosphere of Venus from Pioneer Venus radio occultation data. *Journal of Atmospheric Sciences*, 41:1901–1913, June 1984.

A. Piccialli, D. V. Titov, D. Grassi, I. Khatuntsev, P. Drossart, G. Piccioni, and A. Migliorini. Cyclostrophic winds from the Visible and Infrared Ther-

mal Imaging Spectrometer temperature sounding: A preliminary analysis. *Journal of Geophysical Research (Planets)*, 113(E12), October 2008.

A. Piccialli, S. Tellmann, D. V. Titov, S.S. Limaye, I.V. Khatuntsev, M. Paetzold, and B. Hausler. Zonal thermal winds on Venus derived from the radio-occultation temperature sounding on board Venus Express. *Submitted to Icarus*, 2011.

G. Piccioni, P. Drossart, A. Sanchez-Lavega, R. Hueso, F. W. Taylor, C. F. Wilson, D. Grassi, L. Zasova, M. Moriconi, A. Adriani, S. Lebonnois, A. Coradini, B. Bézard, F. Angrilli, G. Arnold, K. H. Baines, G. Bellucci, J. Benkhoff, J. P. Bibring, A. Blanco, M. I. Blecka, R. W. Carlson, A. di Lellis, T. Encrenaz, S. Erard, S. Fonti, V. Formisano, T. Fouchet, R. Garcia, R. Haus, J. Helbert, N. I. Ignatiev, P. G. J. Irwin, Y. Langevin, M. A. Lopez-Valverde, D. Luz, L. Marinangeli, V. Orofino, A. V. Rodin, M. C. Roos-Serote, B. Saggin, D. M. Stam, D. Titov, G. Visconti, M. Zambelli, E. Ammannito, A. Barbis, R. Berlin, C. Bettanini, A. Boccaccini, G. Bonnello, M. Bouye, F. Capaccioni, A. Cardesin Moinelo, F. Carraro, G. Cherubini, M. Cosi, M. Dami, M. de Nino, D. Del Vento, M. di Giampietro, A. Donati, O. Dupuis, S. Espinasse, A. Fabbri, A. Fave, I. F. Veltroni, G. Filacchione, K. Garceran, Y. Ghomchi, M. Giustini, B. Gondet, Y. Hello, F. Henry, S. Hofer, G. Huntzinger, J. Kachlicki, R. Knoll, K. Driss, A. Mazzoni, R. Melchiorri, G. Mondello, F. Monti, C. Neumann, F. Nuccilli, J. Parisot, C. Pasqui, S. Perferi, G. Peter, A. Piacentino, C. Pompei, J.-M. Reess, J.-P. Rivet, A. Romano, N. Russ, M. Santoni, A. Scarpelli, A. Semery, A. Soufflot, D. Stefanovitch, E. Suetta, F. Tarchi, N. Tonetti, F. Tosi, and B. Ulmer. South-polar features on Venus similar to those near the north pole. *Nature*, 450:637–640, November 2007a.

G. Piccioni, P. Drossart, E. Suetta, M. Cosi, E. Ammannitto, A. Barbis,

R. Berlin, Boccaccini A., G. Bonello, M. Bouye, F. Capaccioni, G. Cherubini, M. Dami, O. Dupuis, A. Fave, G. Filacchione, Y. Hello, F. Henry, S. Hofer, G. Huntzinger, R. Melchiorri, J. Parisot, C. Pasqui, G. Peter, C. Compei, J.M. Reess, A. Semery, A. Soufflot, and the VIRTIS Co-I team. VIRTIS: The Visible and Infrared Thermal Imaging Spectrometer. *ESA SP, 1295*, 2007b.

M. Roos-Serote, P. Drossart, T. Encrenaz, E. Lellouch, R. W. Carlson, K. H. Baines, F. W. Taylor, and S. B. Calcutt. The thermal structure and dynamics of the atmosphere of Venus between 70 and 90 KM from the Galileo-NIMS spectra. *Icarus*, 114:300–309, April 1995.

W. B. Rossow and G. P. Williams. Large-scale motion in the Venus stratosphere. *Journal of Atmospheric Sciences*, 36:377–389, March 1979.

A. Sánchez-Lavega, R. Hueso, G. Piccioni, P. Drossart, J. Peralta, S. Pérez-Hoyos, C. F. Wilson, F. W. Taylor, K. H. Baines, D. Luz, S. Erard, and S. Lebonnois. Variable winds on Venus mapped in three dimensions. *Geophys. Res. Lett.*, 35:13204, July 2008.

J. T. Schofield and D. J. Diner. Rotation of Venus's polar dipole. *Nature*, 305: 116–119, September 1983. doi: 10.1038/305116a0.

G. Schubert. *Venus*, pages 681–765. 1983.

W. H. Schubert, M. T. Montgomery, R. K. Taft, T. A. Guinn, S. R. Fulton, J. P. Kossin, and J. P. Edwards. Polygonal Eyewalls, Asymmetric Eye Contraction, and Potential Vorticity Mixing in Hurricanes. *Journal of Atmospheric Sciences*, 56:1197–1223, May 1999.

A. Seiff. *Venus*, pages 215–279. 1983.

A. Seiff, D. B. Kirk, R. E. Young, R. C. Blanchard, J. T. Findlay, G. M. Kelly, and S. C. Sommer. Measurements of thermal structure and thermal contrasts in the atmosphere of Venus and related dynamical observations

- Results from the four Pioneer Venus probes. *J. Geophys. Res.*, 85:7903–7933, December 1980.

F. W. Taylor, D. J. McCleese, and D. J. Diner. Polar clearing in the Venus clouds observed from the Pioneer Orbiter. *Nature*, 279:613–+, June 1979.

M. G. Tomasko, L. R. Doose, and P. H. Smith. The absorption of solar energy and the heating rate in the atmosphere of Venus. *Advances in Space Research*, 5:71–79, 1985.

D. R. Williams. Venus fact sheet: National space science data center. *http://nssdc.gsfc.nasa.gov/planetary/factsheet/venusfact.html*, 2003.

L. V. Zasova, V. M. Linkin, and I. V. Khatuntsev. Zonal wind in the middle atmosphere of Venus. *Kosmicheskie Issledovaniia*, 38:54–70, February 2000.

L. V. Zasova, N. Ignatiev, I. Khatuntsev, and V. Linkin. Structure of the Venus atmosphere. *Planetary and Space Science*, 55:1712–1728, October 2007.

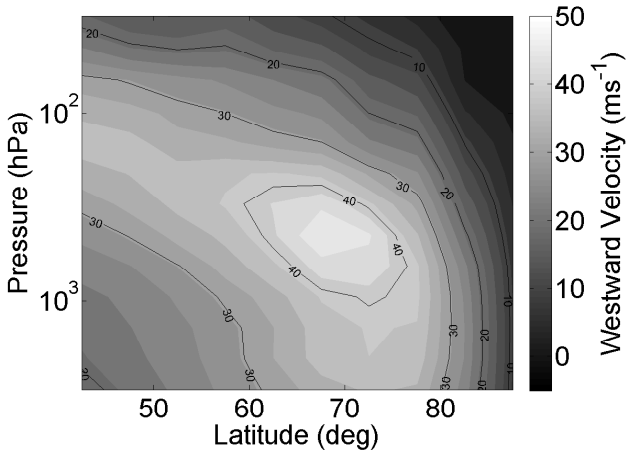

(a) (prograde) Westward Velocity (m/s)

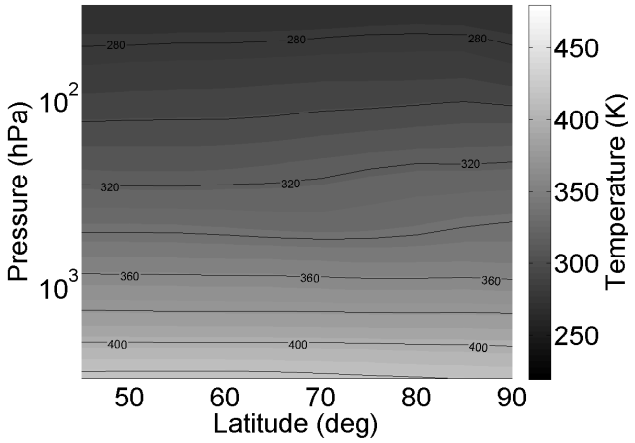

(b) Temperatures (K)

Fig. 1. Zonally and time (one hour) averaged maps calculated by the SGCM, at the end of the model's integration in the North Hemisphere: (**a**) zonal winds; (**b**) temperature map.

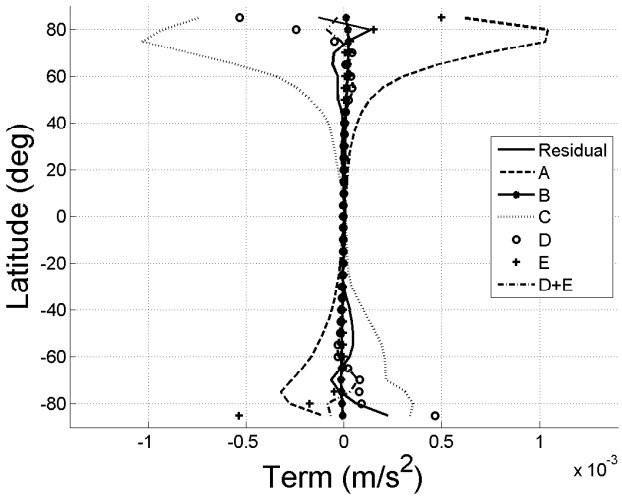

(a) Evaluation at 951 hPa.

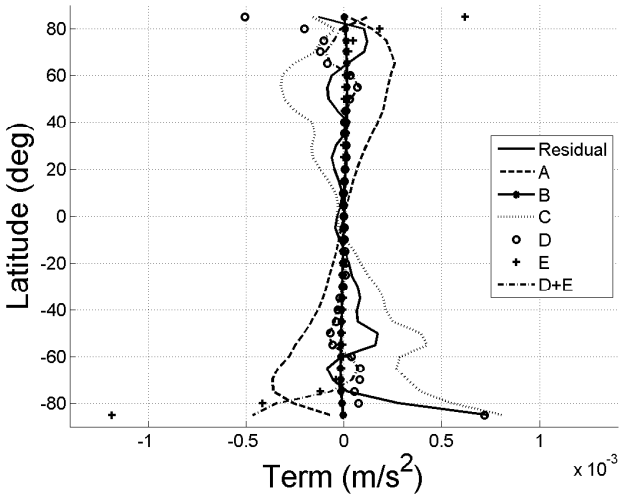

(b) Evaluation at 100 hPa.

Fig. 2. The different lines represent each term of the meridional component of the equation of motion. They were obtained after 4.1×10^5 earth days in the SGCM integration without diurnal forcing. Each term was averaged over longitude and time (1 hour). Note: $A = \frac{u^2 \tan\phi}{a}$, $B = u2\Omega \sin\phi$, $D = \frac{1}{a}\frac{\partial \Phi}{\partial \phi}$, $C = (a\cos\phi)^{-1}(\overline{v'^2}\cos\phi)_\phi$ and $D = \overline{u'^2}a^{-1}\tan\phi$; where ϕ is the latitude and Ω is the rotation rate of the planet.

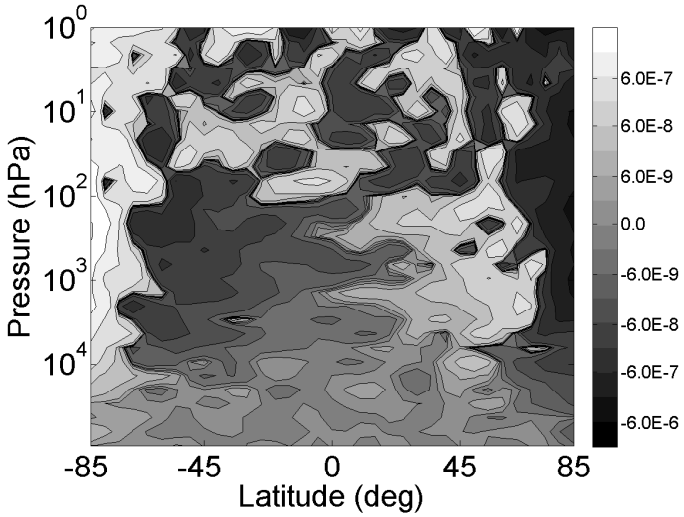

(a) Eddy forcing term: $(a\cos\phi)^{-1}(\overline{v'^2}\cos\phi)_\phi$

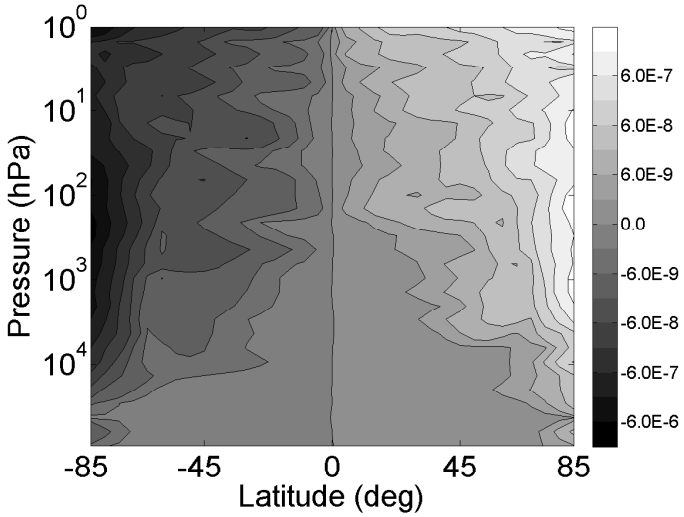

(b) Eddy forcing term: $\overline{u'^2}a^{-1}\tan\phi$

Fig. 3. Eddy terms obtained from Eq. (3) and time averaged for 1 hour. The derivation of these terms are explained in Andrews et al. (1987).

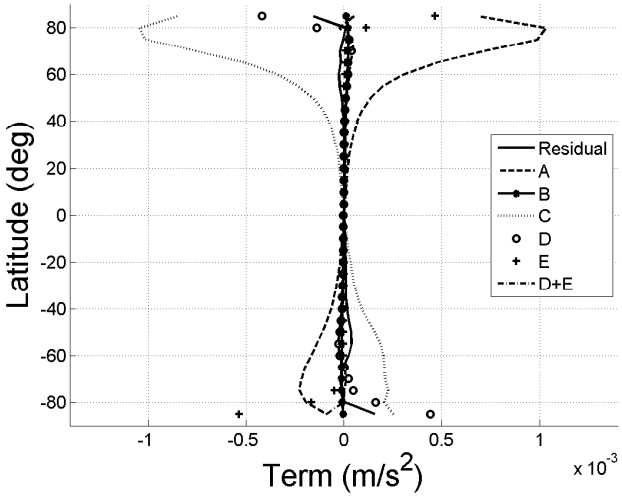

(a) Evaluation at 951 hPa.

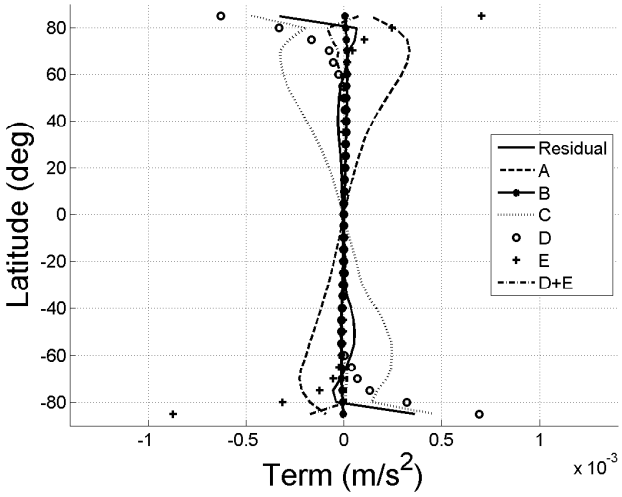

(b) Evaluation at 100 hPa.

Fig. 4. Similar to Figure 2, but time averaging each term for 60 Earth days.

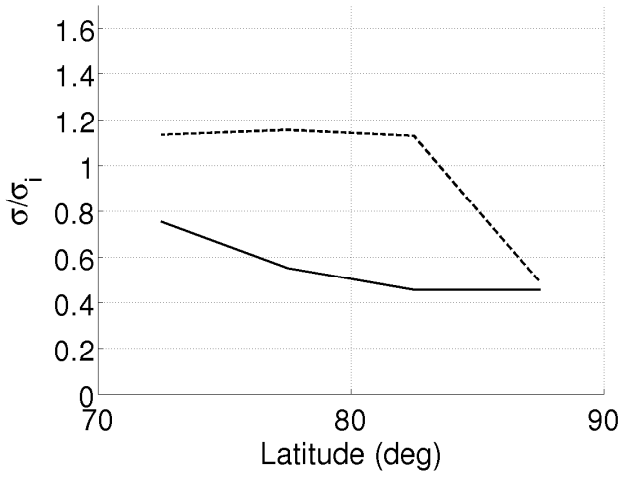

Fig. 5. The dashed line represents the ratio of the standard deviation of the zonal thermal winds at the top of the domain over the standard deviation of the initial guesses. The solid line is the ratio of the standard deviation of the "corrected" top profiles (solid body rotation shape) over the standard deviation of the initial guesses.

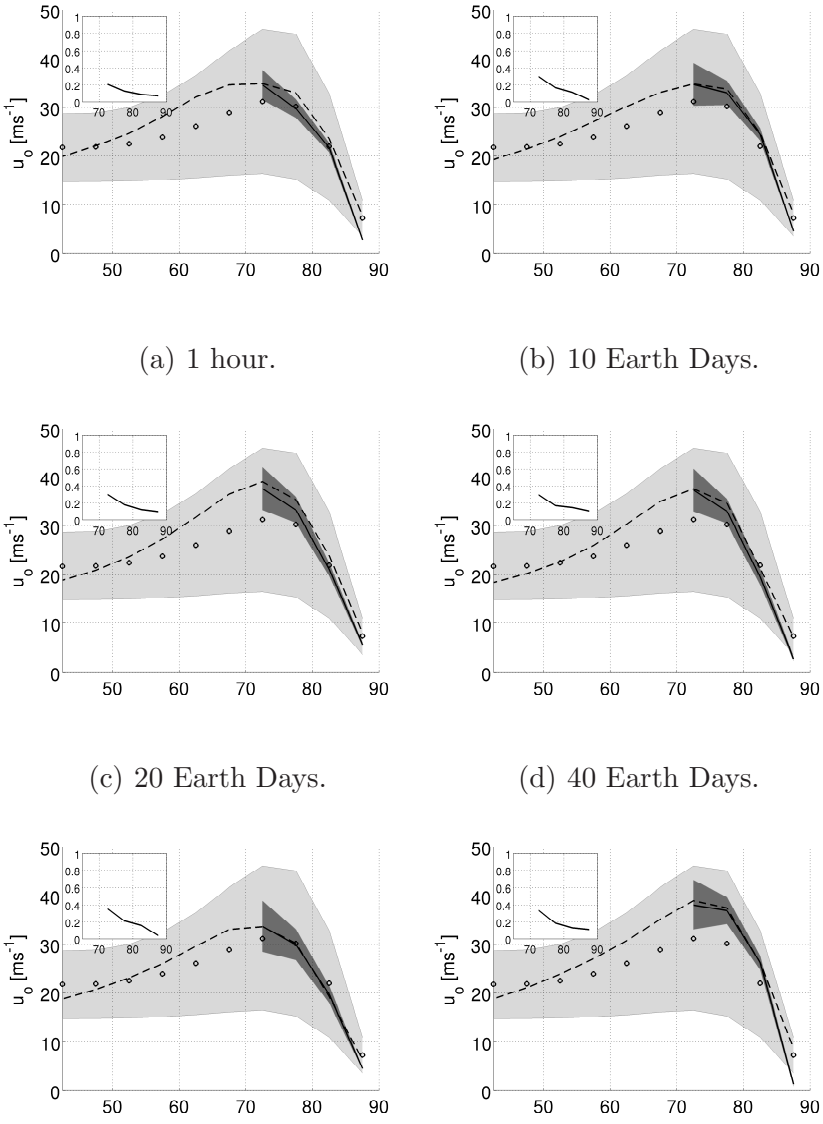

(a) 1 hour. (b) 10 Earth Days.

(c) 20 Earth Days. (d) 40 Earth Days.

(e) 60 Earth Days. (f) 80 Earth Days.

Fig. 6. An ensemble of initial lower boundary profiles is used for six different time averaging periods of the temperature field, applied to the new method to estimate the lower boundary. **(a)** 1 hour, **(b)** 10 Earth days, **(c)** 20 Earth days, **(d)** 40 Earth days, **(e)** 60 Earth days and **(f)** 80 Earth days. The unfilled circles represent the mean of the initial profiles; the dashed line is the actual zonal winds from the SGCM at an altitude where the lower boundary condition is defined, and the solid line is the mean final result. The darker shaded region represents the standard deviation of the final results and the other for the initial guesses. The small plot represents the ratio of the standard deviation of the solid line over the standard deviation of the initial guesses.

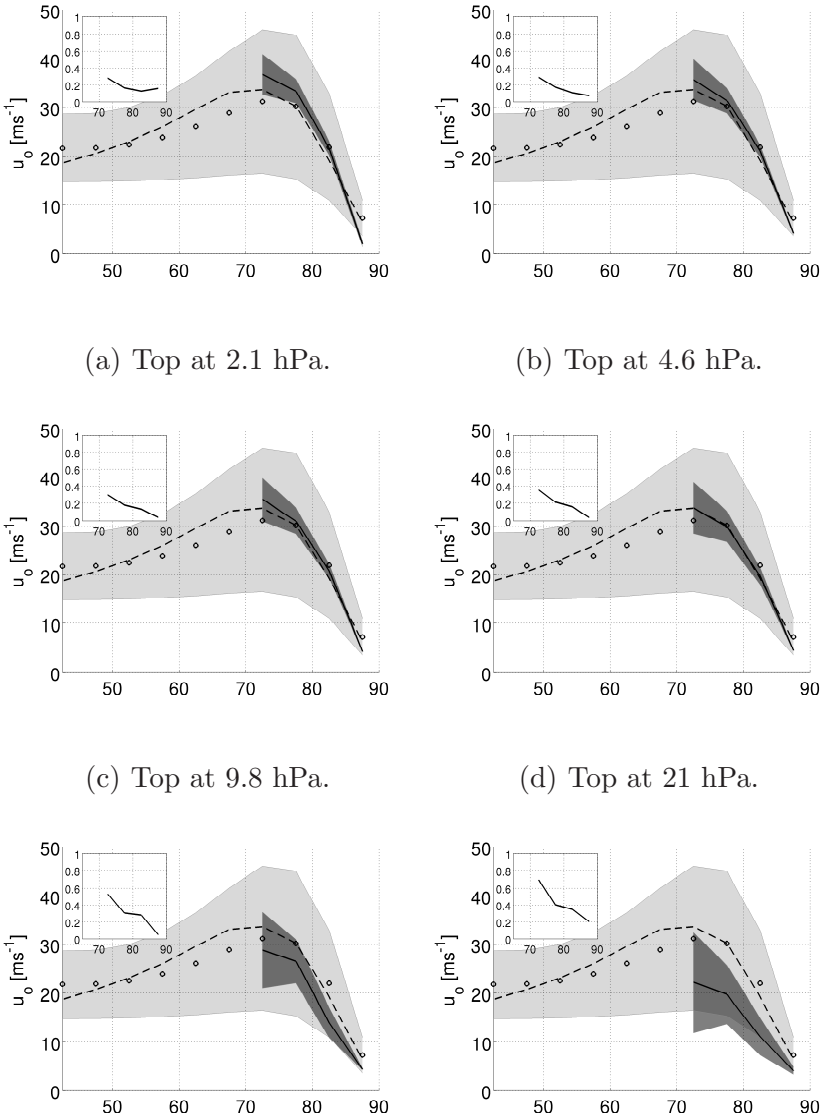

(a) Top at 2.1 hPa.

(b) Top at 4.6 hPa.

(c) Top at 9.8 hPa.

(d) Top at 21 hPa.

(e) Top at 45 hPa.

(f) Top at 100 hPa.

Fig. 7. Similar to Fig. 6. Here we explored the influence of different pressure tops. Six altitudes were chosen to test the method to estimate the lower boundary, applied to: **(a)** 2.1 hPa, **(b)** 4.6 hPa, **(c)** 9.8 hPa, **(d)** 21 hPa, **(e)** 45 hPa and **(f)** 100 hPa. The temperature fields were averaged to 60 Earth days.

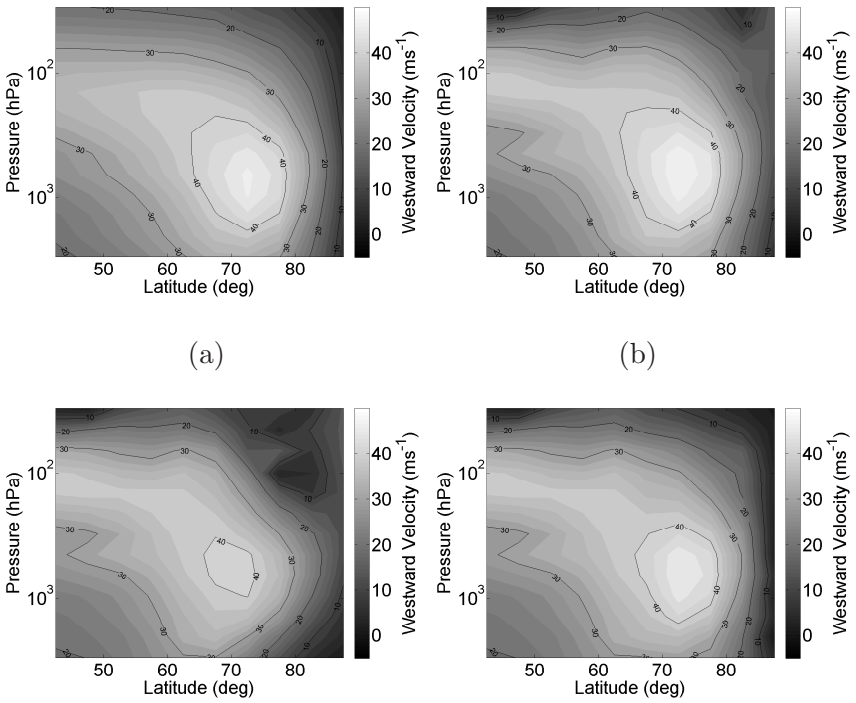

Fig. 8. **(a)** Zonally and time (60 Earth days) averaged zonal winds obtained by the SGCM. **(b)**, **(c)** and **(d)** are thermal zonal winds maps retrieved from the zonally and time averaged (60 Earth days) temperature field obtained by the SGCM. For **(b)**, a zonally and time averaged zonal wind profile obtained by the SGCM was used as lower boundary condition and for **(c)** the Eq. (4) was used instead, with $a = 50\ \mathrm{m\,s^{-1}}$, $b = 70^o$, $c = 10$ and $d = 20\ \mathrm{m\,s^{-1}}$. In **(d)** the thermal zonal winds was obtained applying the method that better estimates the lower boundary condition on case (c).

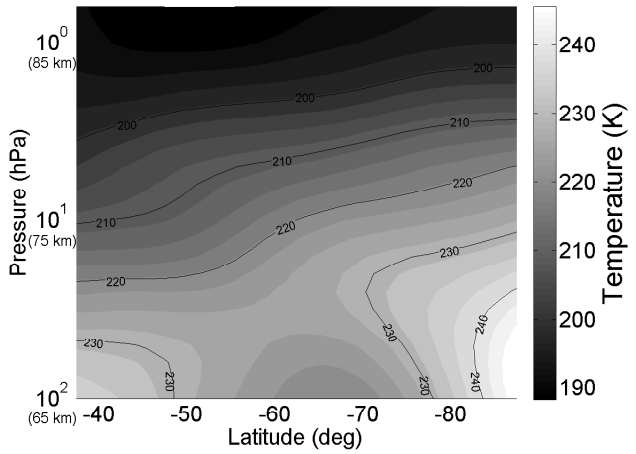

Fig. 9. Temperature map for 2400 LT derived from VIRTIS temperature retrievals (Grassi et al. 2010).

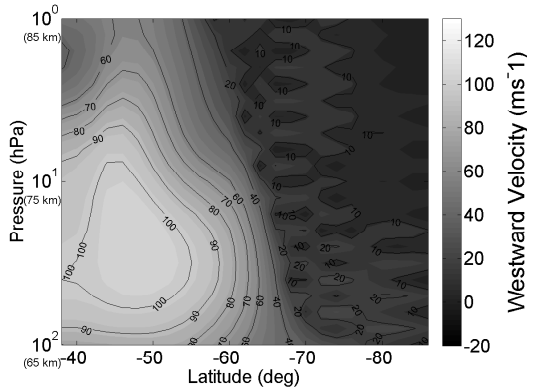

(a)

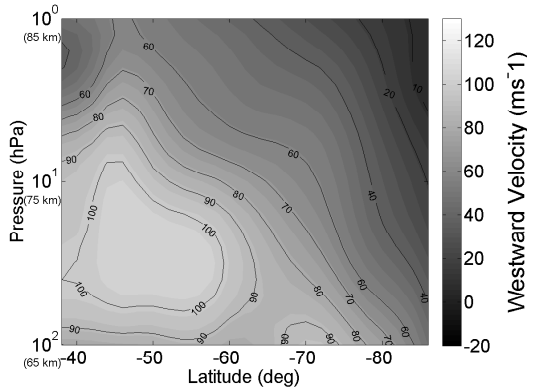

(b)

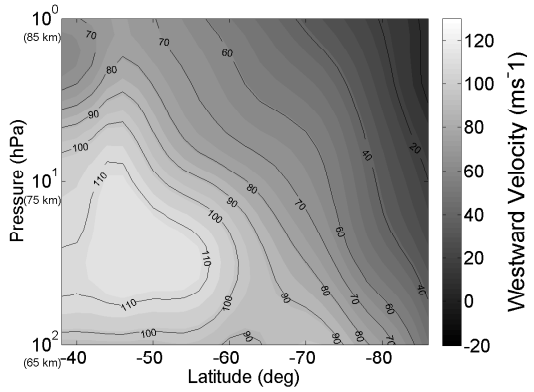

(c)

Fig. 10. (prograde) Zonal thermal wind speed (m/s) derived from VIRTIS 2400 LT temperature field (Grassi et al., 2010) assuming cyclostrophic balance. Figure **(a)** was obtained from the upward integration of the thermal wind equation using for lower boundary the Eq. (4) with $a = 52\ \mathrm{m\,s^{-1}}$, $b = 56^o$, $c = 9$ and $d = 86\ \mathrm{m\,s^{-1}}$. **(b)** and **(c)** use the new method to estimate the lower boundary but different initial guesses. **(b)** uses the same first initial guess as **(a)** for the lower boundary but in **(c)** we use a modified equation with d =105 $\mathrm{m\,s^{-1}}$ instead of d =86 $\mathrm{m\,s^{-1}}$.

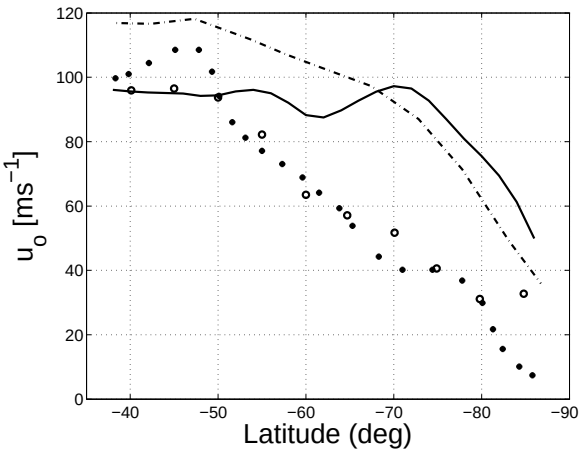

Fig. 11. Comparison between the latitudinal cyclostrophic profiles winds from our new method (solid line) using an initial lower boundary condition that was prescribed to have the form of the Eq. (4) with $a = 52\ \mathrm{m\,s^{-1}}$, $b = 56^o$, $c = 9$ and $d = 86\ \mathrm{m\,s^{-1}}$ and the results from Piccialli et al. (2011) (dashed-dot line) at $\sim 65km$, and the cloud tracked winds from Sánchez-Lavega et al. (2008) at ~ 66 km (black circles) and Moissl et al. (2009) at $\sim 70km$ (unfilled circles).

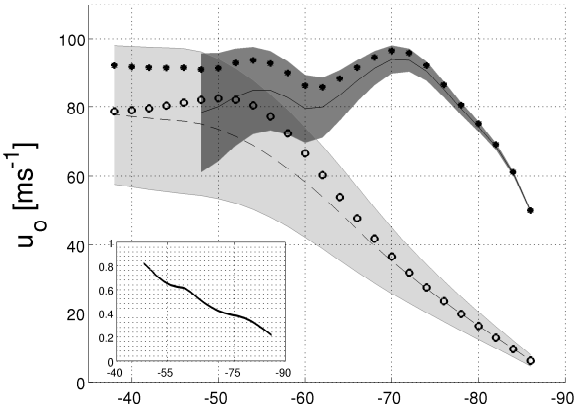

Fig. 12. Similar to Figs. 6 and 7 but now using VIRTIS temperature retrievals (Grassi et al. 2010). The zonal winds are defined in the prograde direction and the lower boundary condition at 100 hPa. The dashed line represents the mean of the initial profiles and the solid line is the mean final result. The darker shaded region represents the standard deviation of the final results and the other for the initial guesses. The small plot represents the ratio of the standard deviation of the solid line over the standard deviation of the initial guesses. The initial lower boundary condition that was prescribed to have the form of the Eq. (4) with $a = 52$ m s^{-1}, $b = 56^o$, $c = 9$ and $d = 86$ m s^{-1} is represented by unfilled circles. The calculated lower boundary condition starting with the Eq. (4) where $a = 52$ m s^{-1}, $b = 56^o$, $c = 9$ and $d = 105$ m s^{-1} is represented with black circles.